



On the use of the Angular Spectrum Method for the evaluation of acoustic metasurfaces

Abdelhalim Azbaid El Ouahabi¹ and Gianluca Memoli¹

¹Department of Informatics, University of Sussex, Brighton, BN1 9QJ, United Kingdom
a.azbaid-el-ouahabi@sussex.ac.uk; g.memoli@sussex.ac.uk

Abstract

Metasurfaces with unit cells at sub-wavelength scale have been successfully used to precisely control and manipulate waves, and applications based on static metasurfaces are on the surge. The design of these metasurfaces, however, often proceeds by trial and error, benchmarking different solutions with finite-elements method (FEM) simulations. This is a batch process, which is not quick enough for the real-time adjustments of sound fields promised by adjustable metamaterials. Here, we present a numerical investigation of sound wave propagation after travelling through a metasurface using the Angular Spectrum Method (ASM). Using different application-focused cases (e.g., focusing, steering, self-bending), we compare the predicted result with the simulated distributions of sound pressure obtained with a commercial FE software. Finally, we present a preliminary discussion on the cost-efficiency of the two approaches and on the perspectives opened by using the ASM as a design tool.

Keywords: Angular spectrum method, acoustic metasurface, wavefront manipulation.

1 Introduction

Acoustic wave manipulation using engineered artificial metamaterials is of paramount significance in acoustics. For many years, though, a family of metamaterials, namely, acoustic metasurfaces, have attracted increasing attention due the advantageous features of a planar profile and subwavelength thickness compared to bulkier meta-structures [1-12]. The uniqueness of these metasurfaces lies in their ability to freely adjust the wave fields impinging or passing through them, due to full control on phase and/or amplitude. Most metasurfaces are realised by assembling subwavelength units, which can collectively be used to produce different phenomena, including beam steering [2,11], beam focusing [12] and self-bending beams [5, 9]. Among the different types of metasurfaces, labyrinthine structures have recently attracted extensive research attention due to their ability to exhibit high refractive indexes, multiple vibration modes inside the labyrinth and, consequently, extraordinary acoustic properties [1,4,5].

In this work, we demonstrate a process that leads to the design of a metasurface (see **Figure 1**), starting from constraints in terms of accessible geometry and frequency of operation (step A). We show how a library of metamaterial bricks can be generated using analytical models [13] (step B) and how the final step of designing a brick-based metasurface is equivalent to analog-to-digital conversion [19], often relying on analytical formulae from the literature (steps C and D in **Figure 1**). The process culminates in the batch verification of the performance of the metasurface using a finite-elements commercial software (e.g. COMSOL Multiphysics) and most of the designer's time is spent on this last step (step E in **Figure 1**). In this work, we focus on optimising the last step of this process and use the open-source Matlab toolbox *k-wave* [14] to compare the propagation after the metasurface using the Angular Spectrum Method (ASM) and a 3D k-space Pseudo-

Spectral Method (PSM), while benchmarking the results with a full finite-elements COMSOL model (FEM). Results show that using ASM is a quick and efficient tool to verify the performance of acoustic metasurfaces in real time adjustments, with potential to be used in the design itself.

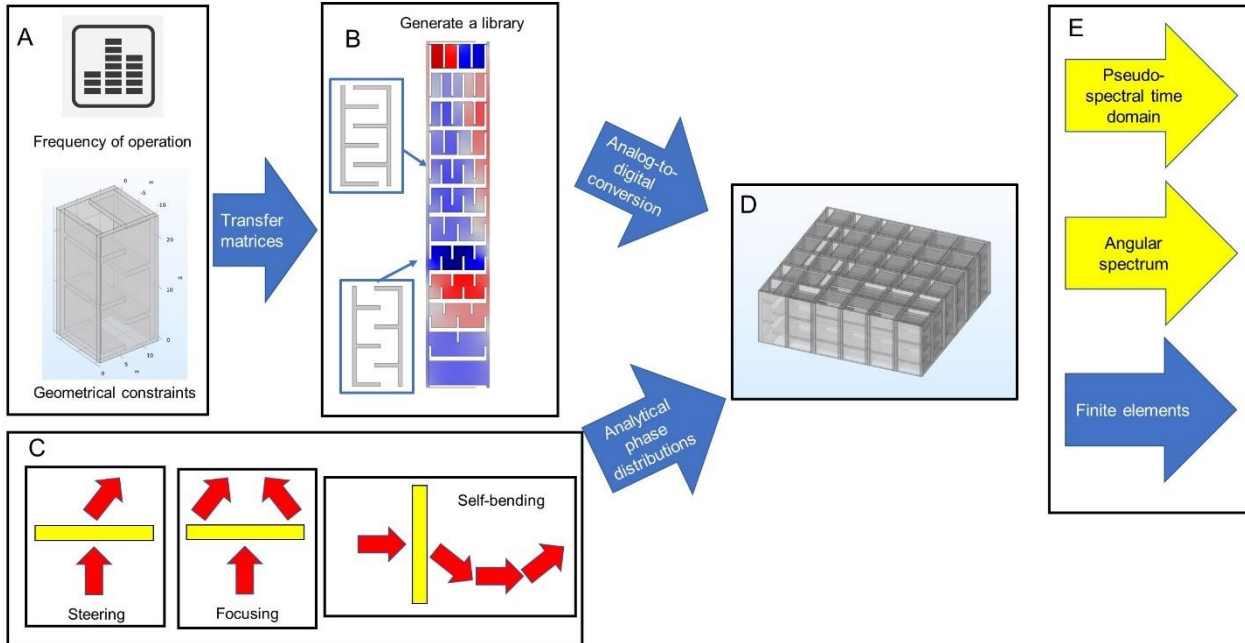


Figure 1. A schematic of the process of designing a metasurface underpinning this work. First, an analytical model based on transfer matrices [13] is used to generate a library of metamaterial bricks (B) from constraints in terms of geometry and frequency operation (A). Analytical phase distributions are then selected from the literature [4, 18] to represent the desired functionalities (C) and used to design (D) a brick-based metasurface [19]. In this work, we compare different numerical methods for propagation (E).

2 Designing a library of bricks

At the start of this work, we decided to use transmittive labyrinthine unit cells for our metasurfaces, like the one in **Figure 1A**, with 1 mm side walls, and set. We set their dimensions to cuboids of size $12.5 \times 12.5 \times 25$ mm, with 25 mm (i.e. 1 inch) in the direction of sound propagation and their main operating frequency to 3430 Hz (wavelength: $\lambda_0 = 100$ mm at ambient temperature). We then parametrised each brick with three numbers: (m, n, l) where m and n are the (integer) number of horizontal bars respectively on the left and right side (of a brick section) and l is their length. All the bars were considered to be identical, with a fixed thickness $w = 1$ mm.

To form the desired fields with optimal performance, the labyrinthine structures units should possess the ability to transmit sound wave effectively, while shifting phases with a 2π range. To check whether this was possible with our geometrical constraints, we adapted to our brick design an analytical model, based on transfer matrices [13], that could give the amplitude and phase shift of the transmitted sound waves as a function of the parameters (m, n, l) . This model assumes a plane wave impinging normal to one side of each brick and no interactions between two adjacent bricks.

The results of this exercise (using Matlab 2021a) can be seen in **Figure 2**, which reports the transmitted amplitude and the phase shift for five types of labyrinthine structure units as a function of the bar length, l , with wavelength, $\lambda = 100$ mm. By changing the parameters (m, n) , it can be observed that the phase shift of the transmitted waves always increases smoothly with the bar length l , but also that the output phase does not cover the full range of $(0, 2\pi)$. It is also noted that, in the region of bar lengths between 8 and 10 mm, the

transmission is considerably reduced. As mentioned in [20], these two considerations reduce the shapes of acoustic field that can be realized with this geometry of bricks.

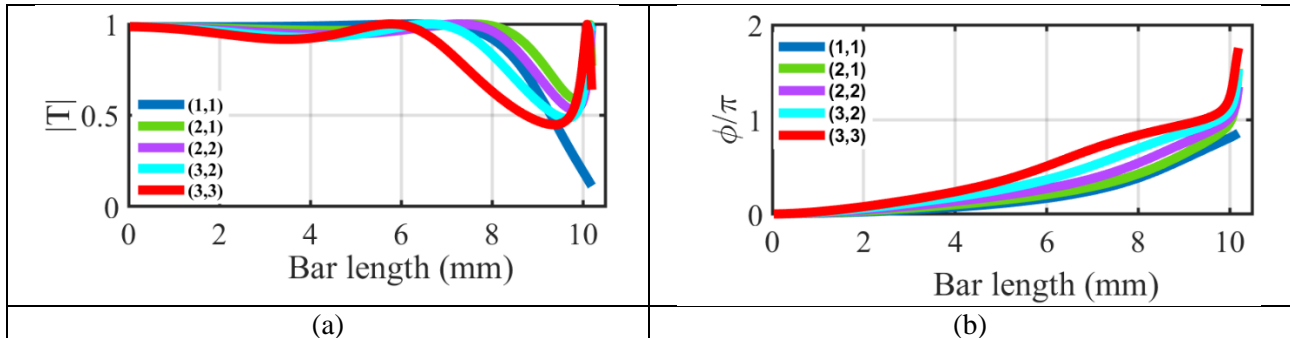


Figure 2. (a) Amplitude and (b) Phase shift of the transmitted waves for five kinds of labyrinthine units as a function of the length l of the bar with wavelength $\lambda = 100$ mm and different combinations of (m, n) .

Nevertheless, following the guidelines in [19], we selected among the many possible combinations of parameters a set of bricks that gave a phase shift in multiples of $\pi/8$ while maximizing the transmission. This gave us 12 brick designs, each encoding a pre-defined phase shift $h \cdot \pi/8$ where $h = 0 \dots 11$. In the following, we will refer to each of these pre-structured designs with its corresponding phase shift – i.e. “brick 7” will give a delay of $\frac{7}{8}\pi$ (see **Figure 1B**).

3 Metasurface design

As hinted in **Figure 1**, in this work we want to compare the performance of three propagation methods (**Figure 1E**) on three different types of metasurfaces: a steering plate, a focusing plate and a self-bending plate (**Figure 1C**). These three shapes were selected because each has the desired phase distribution in analytical form.

3.1 Steering plate

According to the generalized Snell’s law [18], when the phase shift gradient along the interface, $\frac{d\phi}{dx}$, is a nonzero constant, the relation between the transmitted angle, θ , and the phase shift gradient, can be written as:

$$\sin(\theta) = \frac{\lambda}{2\pi} \frac{d\phi}{dx} \quad (1)$$

where λ is the wavelength of the transmitted wave (here: 100 mm).

The generalized Snell’s law implies the possibility of arbitrarily manipulating the directions of transmitted waves by modulating the phase gradient along the metasurface. This is currently achievable by mechanically substituting the brick distribution along the metasurface, but different researchers are looking into automated geometries. Twelve-bricks, with their phase shift from 0 to $\frac{11\pi}{8}$, were selected and arranged for steering the beam to the angle $\theta = 30^\circ$. **Figure 3** shows the theoretical and discretised phase for steering the beam to the desired angle ..

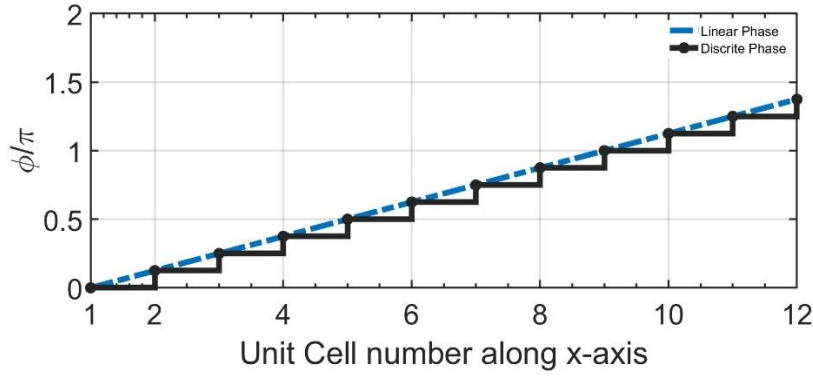


Figure 3. Phase shift along the metasurface used to propagate the beam in the designed angle of 30° . Blue dash-dot line shows the theoretical linear phase shift and solid black line show the discrete phase shift used for the three methods.

3.2 Focusing plate

Due to the full control of the phase profile, the metasurface can be conveniently reconfigured to become an acoustic lens with an arbitrary focal point. To form a focus spot with a focal length F , the phase profile should be expressed as [3]:

$$\phi(x, y) = \frac{2\pi}{\lambda} \left(\sqrt{x^2 + y^2 + F^2} - F \right) \quad (2)$$

For this study, we realised metasurface 12x12 bricks have selected and distributed in 2D for focusing the beam at the desired focal point. Figure 4 shows a theoretical and discrete phase from the metasurface centre along x-axis for focusing the beam at 100 mm.

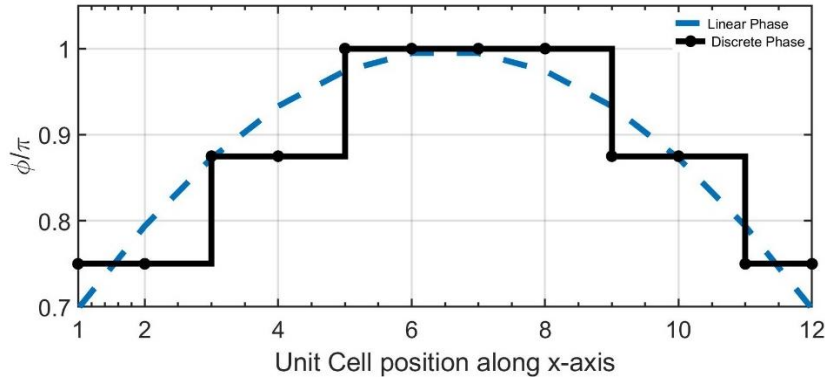


Figure 4. Phase shift from the centre of the metasurface used for beam focusing. Blue dash-dot line shows the theoretical linear phase shift and solid black line show the discrete phase shift used for the three methods.

3.3 Self-bending plate

For the last example in this work, we designed a metasurface with 40 x 40 bricks, imposing on it has been used for generating such a bending beam, and the phase profile provided by the metasurface should be written as [4]

$$\phi(y) = k \left(y - 2r \sqrt{\frac{y}{r}} \right) \quad (3)$$

Where r is the centre of the trajectory of bending.

Figure 5 shows the theoretical and discrete phase used for self-bending of the beam.

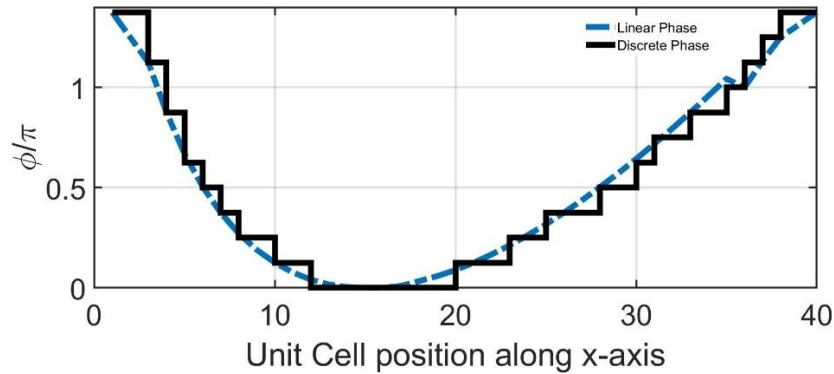


Figure 5. Phase shift along the metasurface used for self-bending. Blue dash-dot line shows the theoretical linear phase shift and solid black line show the discrete phase shift used for the three methods.

4 Theory

In this work, we compare three different modelling (i.e. PSM, ASM and FEM) of sound wave propagation after travelling through a metasurface. Unless otherwise specified, calculations were performed using Matlab 2018.

4.1 k-space Pseudo-Spectral time domain Method

The PSM method [14,15] is a time-stepping scheme for full wave acoustic simulations. This method is widely used as a wave equation solver, for example in the k-wave implementation [16], because of its computation efficiency. Spatial gradients are computed using a spectral method, while temporal gradients are computed using forward differences. This method has advantages over the finite difference time domain and finite element methods due to the reduced number of grid points needed per wavelength to reach convergence (i.e. typically two grid points per wavelength, compared to the six grid points per wavelength needed for FEM).

4.2 Angular Spectrum Method

The angular spectrum method is a technique for monochromatic modelling of a propagating wave field. The technique can predict an acoustic pressure field distribution over a plane, based upon knowledge of the pressure field distribution at a parallel plane, perpendicular to the direction of propagation as shown in Figure 6.

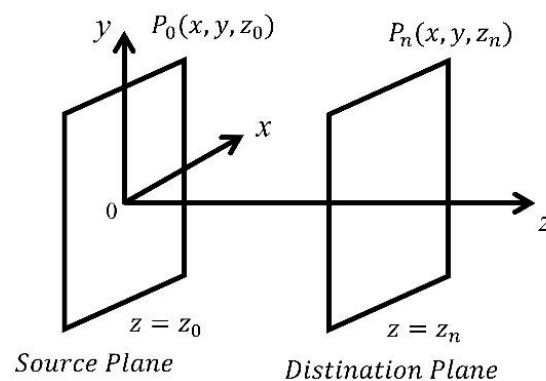


Figure 6. Definition of the coordinate system and the geometry of the ASM.

In Figure 6, $P_0(x, y)$ is the known sound pressure at the source plane – at coordinate z_0 – and we wish to determine the pressure distribution P_n at coordinate z_n along the propagation direction. This can be formulated as [17]:

$$P_n(x, y, z_n) = F^{-1}\{\hat{P}_0(k_x, k_y, z_0)e^{-jk_z(z_n-z_0)}\} \quad (4)$$

where $F^{-1}\{\}$ represents the inverse Fourier transfer, and $\hat{P}_0(k_x, k_y, z_0)$ is a 2D spatial Fourier transform of the source pressure given by

$$\hat{P}_0(k_x, k_y, z_0) = \iint P_0(x, y, z_0)e^{-j(k_x x + k_y y)} dx dy \quad (5)$$

and k_x , k_y and k_z are the wave numbers along the respective axes. It is easy to see that

$$k_z = \pm \sqrt{k^2 - k_x^2 - k_y^2}, \quad (6)$$

where $k = \frac{\omega}{c}$ is the angular frequency ω divided by the sound speed c .

4.3 COMSOL Multiphysics

For the purposes of this work, we have developed a COMSOL model of the different brick configurations, using the Acoustic Module and starting from the basic units generated in Figure 1B. The model was 2D for steering and self-bending, which have an inherent 2D profile, but had to move to 3D when the lens to ensure focusing with the lens assembly. All the models assumed a plane wave impinging perpendicularly on the metasurface. Only half of the metasurface was simulated, in the case of the lens, to exploiting its symmetries.

5 Results and discussion

The open-source k-Wave Toolbox was used to compute wave propagation using a continuous wave source for each cell unit constituting the metasurface, with the phase shift predicted by generalized Snell's law for steering, focusing or self-bending the wavefront. The amplitude has been determined from the Fig. 2(a) which correspond to the phase shift selected for cell units. The Angular Spectrum Method was used to project the pressure distributions over the metasurface to another parallel plane to the metasurface by using t

5.1 Acoustic beam steering

A 12x12 brick assembly, providing a discrete phase profile that resembles the desired linearly gradient phase profile, $\phi(y) = k \sin(\theta)y$, has been used for beam steering, where θ is the desired beam angle ($\theta = 30^\circ$ herein) and k is the wavenumber of the wave propagation. In order to calculate its performance, the angle of deviation of the beam was calculated at different distances from the metasurface and the simulated angles of deviation for ASM and FEM have been shown in Figure 7.

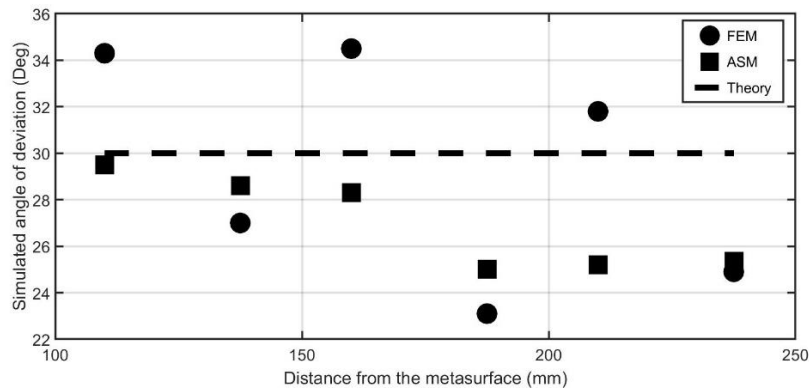


Figure 7. Simulated angle of deviation at different distances from the metasurface.

At most distances, ASM presents good results in comparison with FEM. At 110 mm the angle of deviation is very close to the theory, which gives 29° . It should be observed that, when the distance from the metasurface increases, the angle of deviation moves away from the theoretical angle.

5.2 Acoustic beam focusing

As mentioned previously, 12x12 bricks have been used for the beam focusing metasurface. Figures 8 and 9 show a normalized pressure, along the 2D-Colour presentation of the pressure for the three methods at the focal point, 100 mm. Results show good agreement between the three methods, but in terms of computation the ASM proved to be faster than the other two methods.

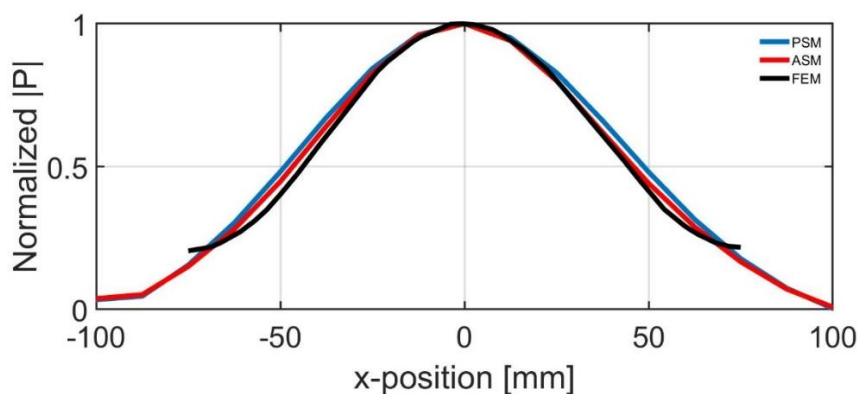


Figure 8. Normalized pressure along the x-axis at the focal point $F=100$ mm.

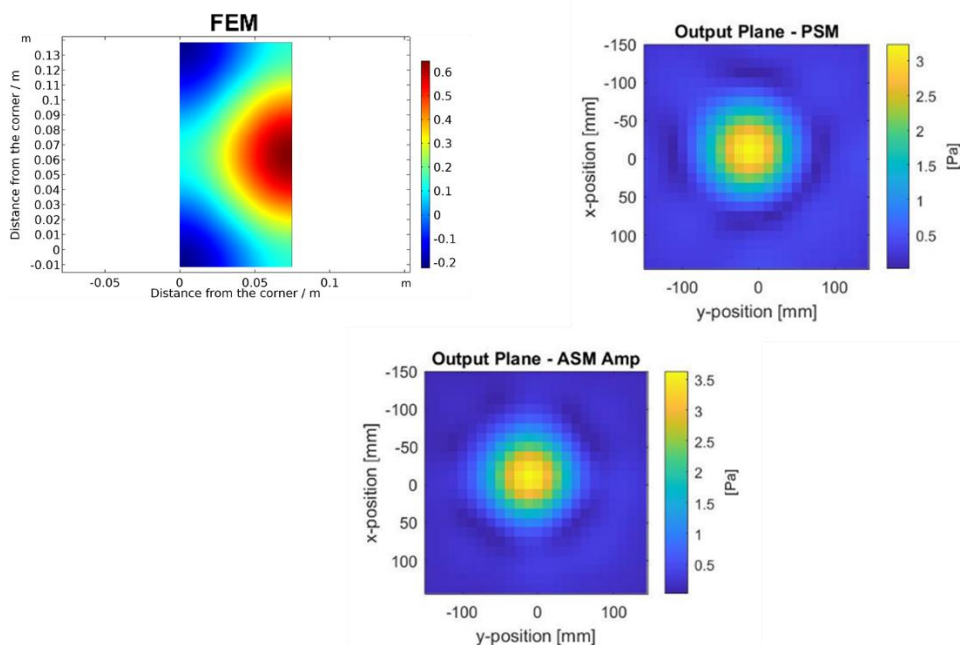


Figure 9. 2D-Colour presentation of the field distribution at the focal point 100 mm. Half of 2D-colour presentation presented for FEM. Left top plot by PSM and the bottom by ASM.

5.3 Acoustic beam self-bending

To produce a self-bending of the beam, a larger metasurface than the other cases, 40x40 bricks, has been used. This choice was necessary, to capture within the metasurface both the part creating the lower part of the bend and the other, closing the trajectory. A 2D colour representation of the pressure along the z-axis (and therefore calculated using the PSM) is shown in Figure 10.

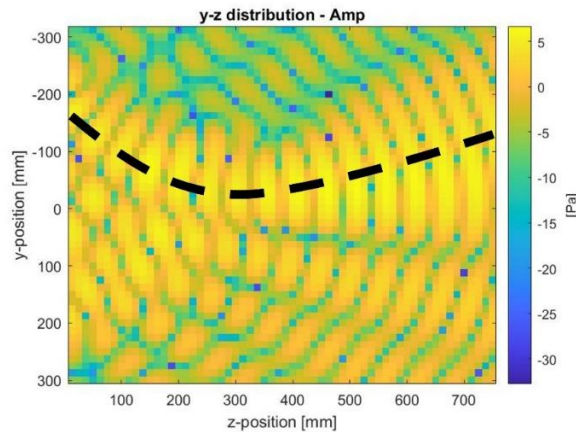


Figure 10. 2D-Colour presentation of the sound pressure along the z-axis using the PSM.

Results in Figure 10 show a self-bending of the beam along the designed arc trajectory. The same self-bending was obtained by ASM, as shown in Figure 11. Since ASM (in *k-wave*) is designed to project on parallel planes, a slicing visualisation has been used in Figure 11.

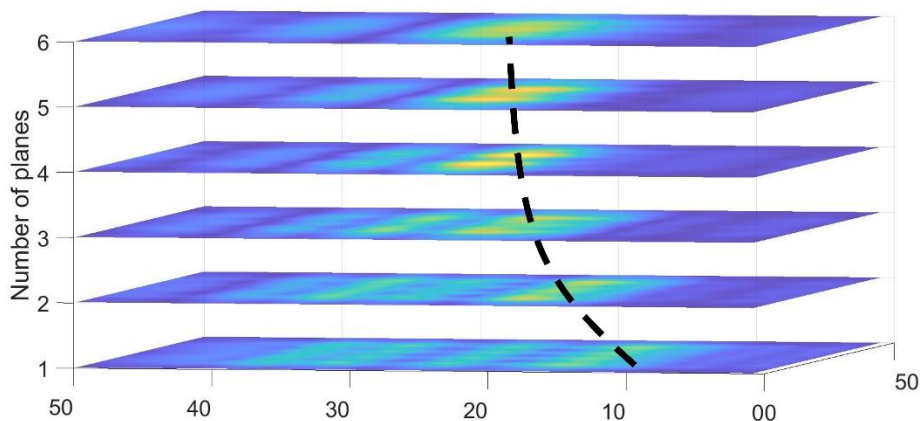


Figure 11. 2D-Colour presentation of the sound pressure at various distances from the metasurface in the range 50 mm to 500 mm, using the ASM. The vertical axis shows the number of the plane.

6 Conclusions

A numerical investigation of sound wave propagation after travelling through a metasurface using the ASM, PSM and FEM has been presented in this work, for steering, focusing and self-bending of the beam. ASM shows a good agreement, when compared with both the FEM and the PSM, and is quicker than FEM in terms of computation time. This method should be an efficient tool for visualising the real-time adjustments of sound fields required by adjustable metamaterials. One of the further advantages of using the angular spectrum is that it can be inverted: given a desired pressure distribution, it can be used to back-propagate the field to the metasurface, thus determining how the metasurface has to sculpt the impinging wave. For some simple cases,

like the ones in this study, this may lead to AI-driven metasurface design: a possibility that will be assessed in future studies.

Acknowledgements

The authors acknowledge funding from the Engineering and Physical Sciences Research Council (EPSRC-UKRI) through project AURORA-EP/S001832/1

References

- [1] Li, Y., Liang, B., Gu, Z. M., Zou, X. Y. & Cheng, J. C. Reflected wavefront manipulation based on ultrathin planar acoustic metasurfaces. *Sci. Rep.* 3, 2546 (2013).
- [2] Li, Y., Jiang, X., Liang, B., Cheng, J. C. & Zhang, L. Metascreen-based acoustic passive phased array. *Phys. Rev. Appl.* 4, 024003 (2015).
- [3] Li, Y. et al. Theory of metascreen-based acoustic passive phased array. *New J. Phys.* 18, 043024 (2016).
- [4] Yong Li et al. Experimental realization of full control of reflected waves with subwavelength acoustic metasurfaces. *Phys. Rev. Appl.* 2, 064002 (2014).
- [5] Xie, Y. et al. Wavefront modulation and subwavelength diffractive acoustics with an acoustic metasurface. *Nat. Commun.* 5, 5553 (2014).
- [6] Mei, J. & Wu, Y. Controllable transmission and total reflection through an impedance-matched acoustic metasurface. *New J. Phys.* 16, 123007 (2014).
- [7] Zhu, X. et al. Implementation of dispersion-free slow acoustic wave propagation and phase engineering with helical-structured metamaterials. *Nat. Commun.* 7, 11731 (2016).
- [8] Al Jahdali, R. & Wu, Y. High transmission acoustic focusing by impedance matched acoustic metasurfaces. *Appl. Phys. Lett.* 108, 031902 (2016).
- [9] Li, Y. & Assouar, M. B. Three-dimensional collimated self-accelerating beam through acoustic metascreen. *Sci. Rep.* 5, 17612 (2015).
- [10] Jiang, X., Li, Y., Liang, B., Cheng, J. & Zhang, L. Convert acoustic resonances to orbital angular momentum. *Phys. Rev. Lett.* 117, 034301 (2016).
- [11] Li Cai, Jihong Wen, Dianlong Yu, Zhimiao Lu, Xing Chen, and Xiang Zhao. Beam steering of the acoustic metasurface under a subwavelength periodic modulation, *Appl. Phys. Lett.* 111, 201902 (2017).
- [12] Di-Chao Chen,¹ Xing-Feng Zhu,^{1,2,a} Qi Wei,¹ Da-Jian Wu,^{1,a} and Xiao-Jun Liu². Broadband acoustic focusing by Airy-like beams based on acoustic metasurfaces, *Journal of Applied Physics* 123, 044503 (2018).
- [13] Abdelhalim Azbaid El Ouahabi, Letizia Chisari and Gianluca Memoli. Analytical and experimental investigation of the transmission/reflection coefficient from labyrinthine metamaterials. *Proceedings of Meetings on Acoustics*, Vol. 42, 065003 (2020).
- [14] B. E. Treeby and B. T. Cox, "k-Wave: MATLAB toolbox for the simulation and reconstruction of photoacoustic wave-fields," *J. Biomed. Opt.*, vol. 15, no. 2, p. 021314, (2010).
- [15] T. D. Mast, L.P. Souriau, D.-L.D. Liu, M. Tabei, A.I. Nachman, and R.C. Waag, "A k-space method for large-scale models of wave propagation in tissue," *IEEE Trans. Ultrason. Ferroelectr. Freq. Control*, vol. 48, pp.341-354, (2001).
- [16] See <http://www.k-wave.org> (Last viewed 17 September 2020).

- [17] J. W. Goodman, Introduction to Fourier Optics, McGraw-Hill, New York, (1996).
- [18] Yu N, Genevet P, KatsMA, Aieta F, Tetienne J P, Capasso F and Gaburro Z 2011 Light propagation with phase discontinuities: generalized laws of reflection and refraction. Science 334, pp. 334-337, (2011).
- [19] Memoli G., et al. Metamaterial bricks and quantization of meta-surfaces, Nature Communications, 8:14608 | DOI: 10.1038/ncomms14608, (2017).
- [20] Memoli G., Chisari L. et al, VARI-SOUND: A Varifocal Lens for Sound, CHI '19: Proceedings of the 2019 CHI Conference on Human Factors in Computing Systems May, No.: 483, pp 1–14, (2019). <https://doi.org/10.1145/3290605.3300713>